# Investigation of a Novel Solar Assisted Water Heating System with Enhanced Energy Yield for Buildings

Xingxing. Zhang*[1], Xudong Zhao[1], Jihuan Xu[2] and Xiaotong Yu[3]

[1] *Institute of Energy and Sustainable Development, De Montfort University, UK*
[2]*Shanghai Pacific Energy Centre, Shanghai, China*
[3]*Shanghai Solar Energy Research Centre, Shanghai, China*

Email: x.zhang@dmu.ac.uk

**Abstract:**
This paper presented the concept, prototype application, operational performance and benefits relating to a novel solar assisted water heating system for building services. It was undertaken through dedicated theoretical analysis, computer simulation and experimental verification. The unique characteristic of such system consists in the integrated loop heat pipe and heat pump unit (LHP-HP), which was proposed to improve solar photovoltaic (PV) generation, capture additional solar heat, and therefore enhance overall solar energy yield. The evaluation approaches derived from the first-law thermodynamics and the standard/hybrid system performance coefficients ($COP$/$COP_{PV/T}$) were developed for the comprehensive assessments. Under the featured weather conditions, the mean electrical, thermal and overall energetic efficiencies of the module were tested around 9.12%, 38.13% and 47.25% respectively. Whilst the $COP$ and $COP_{PV/T}$ values of entire system were measured at about 5.51 and 8.81 averagely. Moreover, a general comparison of this prototype system against the conventional solar/air energy systems was simply discussed.

**Keywords:**
Efficiency; *COP*; Heat pump; Loop heat pipe; PV;

## 1. Introduction

In EU, building sectors account for approximately 40% of the primary energy consumption and 36% of total carbon emission [EU statistical pocket book 2007/2008]. Improving the building energy efficiency shall provide a substantial contribution towards attaining the EU's energy 'decarburization' targets. To achieve this goal, the high fraction of locally available renewable energy sources in energy mix will become necessary to achieve a significantly reduced energy dependence of buildings. Solar energy is normally regarded as the most important renewable energy source for local heat/cold or power production. The solar assisted building services engineering could be potential solutions for both enhanced energy performance and reduced operating cost in contemporary built environment. To accelerate the process, improving the overall solar conversion efficiency is regarded as the top priority in solar technology innovation and building services. It is recognized that the PV's efficiency falls with its cells temperature rise [Zondag et al., 2002]. To control the cell temperature, the measures were applied to remove the accumulated heat from the PV back surface and further to make utilization of the additional heat for servicing buildings. These approaches, known as PV/Thermal (PV/T) technology, have been proven effectively in increasing solar conversion ratio and making economic use of the solar energy in buildings.

In recent years, numerous researchers has made efforts to develop various PV/T technologies including those by air, water, refrigerant and heat pipe [X Zhang et al., 2012], whose research results indicated the excellent effectiveness of the PV/T devices in increasing solar energy yield. However, use of these PV/T devices has also discovered several inherent technical shortfalls, e.g., low thermal capacity of the media, risk of leakage, uneven heat distribution, and hazard of potential freezing. To overcome these, a unique loop heat pipe structure with the top positioned three-ways tube was initiated. This structure, in combination with the PV layer, can form a modular PV/T collector. This loop-heat-pipe based PV/T type may have potential to overcome the difficulties existing in above systems and have the advantages lying in: (1) efficient thermal performance for a distant travel; (2) hermetically sealed vessel without risk of fluid leakage; (3) homogeneous built-in capillary force leading to even heat distribution; (4) availability for use of anti-freezing liquid; (5) top feeding structure to avoid 'dry-out' problem of the upper liquid film in conventional heat pipes [A. Faghri, 1995].When combining the operation of heat pump, it's therefore expect to achieve highly efficient heat and electricity generation using solar energy.

## 2. System description

The proposed photovoltaic/loop-heat-pipe heat pump (PV/LHP-HP) water heating system is schematically shown in Fig. 1. This system comprises a modular PV/LHP solar collector, an electricity control/storage unit, vapour/liquid transportation lines, a flat-plate heat exchanger acting as the condenser of the heat pipe and the evaporator of heat pump cycle, a hot water tank embedded with a coil-type condenser, a compressor, and an expansion valve.

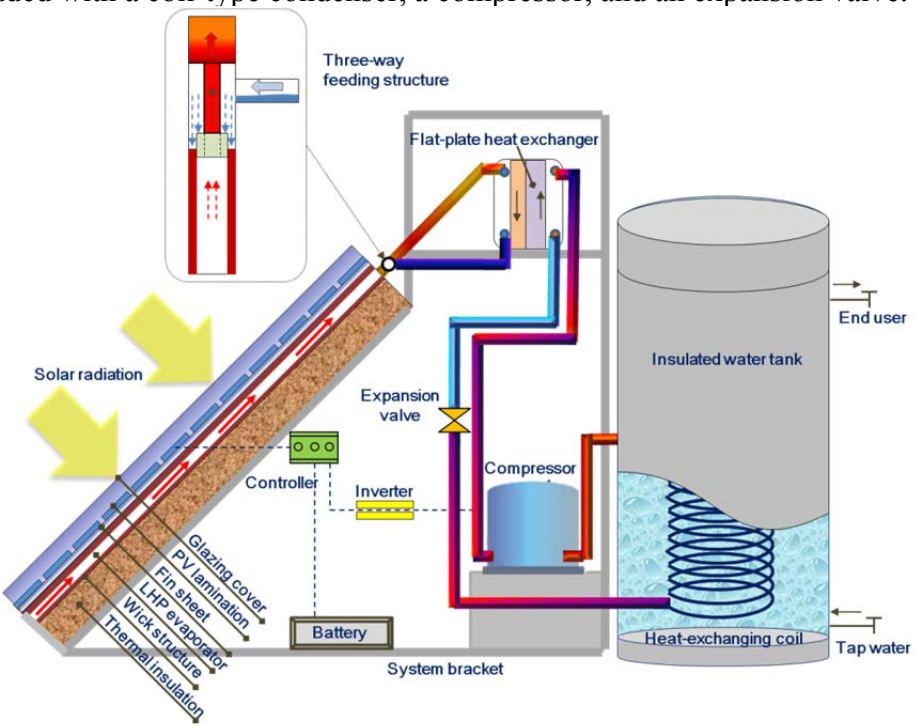


Fig. 1: Schematic of the PV/LHP heat pump system

The LHP evaporator in Fig.1 is an externally finned and internally wicked heat pipe with the three-way tube on the top. This pipe structure could deliver evenly distributed water film across the heat pipe wall from the top, and keep constant saturation of the wall all the way downside, thus preventing the 'dry-out' potential of the water across the wall. The three-way tube, meanwhile, could also deliver the vapour upward to the flat-plate exchanger through the

vapour transportation line. This will create a clear separation between the liquid and vapour flows within the heat pipe. In the module, the LHP evaporator is placed underneath the PV layer to extract heat from the PVs. During the operation, this part of heat will be delivered to the heat exchanger through vapour transportation line, within which heat transfer between the heat pump refrigerant and heat pipe working fluid will occur. This interaction will lead to condensation of the heat pipe working fluid and subsequently the condensed liquid will return to the LHP evaporator via the liquid transportation line, thus completing the heat pipe fluid circulation. Meanwhile in the heat pump cycle, the liquid refrigerant will be vaporized in the heat exchanger, which, driven by the compressor, will be then upgraded into higher pressured, supersaturated vapour, and further release heat into the tank water via the coil exchanger, leading to temperature rise of the tank water. Also, the heat transfer within the coil exchanger will lead to condensation of the high pressured vapour, which, passing via the expansion valve, will be downgraded to the low pressure liquid refrigerant. This refrigerant will undergo the evaporation process within the heat exchanger, thus completing the entire process of heat pump cycle. The ideal thermodynamic process of the refrigerant is shown in Fig. 2.

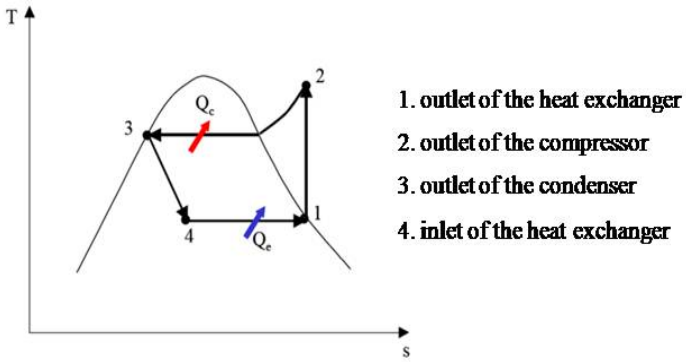


Fig. 2: Indication of the ideal heat pump thermodynamic cycle

The distinct features of the PV/LHP-HP system lie in (1) temperature of the LHP working fluid could be controlled to a lower level through adjustment of the refrigerant evaporation pressure in the heat pump; this will lead to the reduced PV cells temperature, improved module electrical and thermal efficiencies, and increased solar output per unit of absorbing surface; (2) refrigerant temperature/pressure can be raised up to a given level, enabling heat to be transferred from the refrigerant to the tank water; (3) electricity required for driving the compressor can be further delivered from the PV power when designing appropriately, thus creating a near-to-zero-carbon water heating operation. It can be predicted that more or less electricity surplus or deficiency may occur, which can be balanced through the battery storage or connection to the national grid. This system may be installed on a building where the PV/LHP modules could be attached to its façade or roof. For this application, the heat exchanger could be positioned at the upper side of the modules, while the heat pump cycle installed inside of the building. Alternatively, this system can also be separately installed as an independent heat and power generation unit when necessary.

## 3. Mathematical analysis

For this system, the transient mathematical model involves six energy balance equations (Fig. 3): (i) heat balance equation of the glazing cover; (ii) heat balance equation of the PV lamination; (iii) one-dimensional unsteady-sate heat conductance of the fin sheet; (iv) heat balance equation of the loop heat pipe operation; (v) heat balance equations of the heat pump cycle and (vi) water tank.

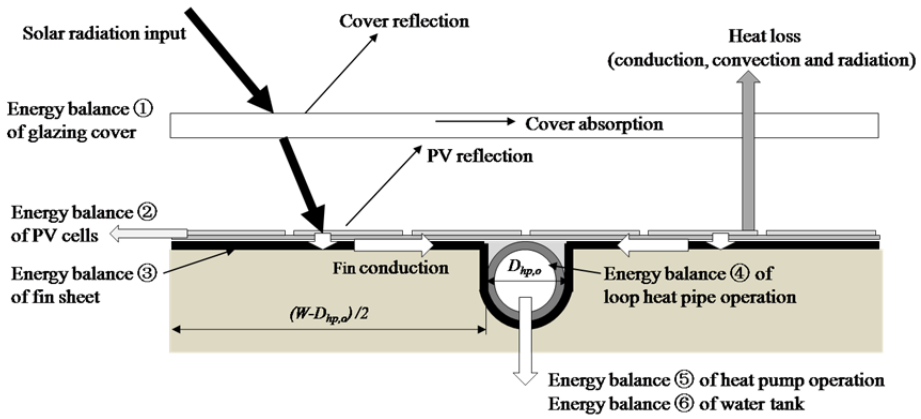


Fig. 3: Schematic of the energy balances involving in the system

### *3.1. Heat balance equation of the glazing cover*

To describe the time dependency of heat flows on a single glazing cover, the corresponding energy balance equation is given by

$$\rho_c c_c \delta_c \frac{\partial T_c}{\partial \tau} = I\alpha_c + \left(h_{c,p-c} + h_{R,p-c}\right)\left(T_p - T_c\right) - \left(h_{c,c-a} + h_{R,c-a}\right)\left(T_c - T_a\right) \tag{1}$$

$$h_{c,p-c} = \frac{k_a}{\delta_a}\left\{1 + 1.446\left(1 - \frac{1708}{Ra_a \cos\theta}\right)^{+}\left[1 - \frac{1708\sin(1.8\theta)^{1.6}}{Ra_a \cos\theta}\right] + \left[\left(\frac{Ra_a \cos\theta}{5830}\right)^{0.333} - 1\right]^{+}\right\} \tag{2}$$

$$Ra_a = \frac{g\left(T_p - T_c\right)\delta_a^{\,3}}{\nu_a^{\,2} T_{a,m}}\mathrm{Pr}_a \tag{3}$$

$$T_{a,m} = \left(T_p + T_c\right)/2 \tag{4}$$

$$h_{R,p-c} = \frac{\sigma\left(T_p + T_c\right)\left(T_p^{\,2} + T_c^{\,2}\right)}{\left(1/\varepsilon_p\right) + \left(1/\varepsilon_c\right) - 1} \tag{5}$$

$$h_a = h_{c,c-a} = \frac{8.6V^{0.6}}{L^{0.4}} \tag{6}$$

$$h_{R,c-a} = \varepsilon_c \sigma\left(T_c + T_s\right)\left(T_c^{\,2} + T_s^{\,2}\right) \tag{7}$$

$$T_s = 0.0552 T_a^{1.5} \tag{8}$$

### *3.2. Heat balance equation of the PV lamination*

The energy balance equation on the combined PV lamination can be written as

$$\rho_p c_p \delta_p \frac{\partial T_p}{\partial \tau} = \left[ I(\tau_c \alpha)_b (1-\beta_p) + I(\tau_c \alpha)_p \beta_p - Q_e \right] - (T_p - T_f) / R_{p-f} A_p - \left( h_{c,p-c} + h_{R,p-c} \right)(T_p - T_c) \tag{9}$$

The overall transient solar transmittance for a single cover becomes

$$\tau_c = \frac{\tau_{c,\alpha}}{2} \left\{ \frac{1-r_{\parallel}}{1+r_{\parallel}} \left[ \frac{1-r_{\parallel}}{1-\left(r_{\parallel}\tau_{c,\alpha}\right)^2} \right] + \frac{1-r_{\perp}}{1+r_{\perp}} \left[ \frac{1-r_{\perp}}{1-\left(r_{\perp}\tau_{c,\alpha}\right)^2} \right] \right\} \tag{10}$$

$$\tau_{c,\alpha} = e^{\left( -\frac{K\delta_c}{\cos(\theta_2)} \right)} \tag{11}$$

$$\theta_2 = \sin^{-1}\left( \frac{\sin\theta_1}{n_g} \right) \tag{12}$$

$$\cos(\theta_1) = \sin(L_m - \theta)\sin(\delta_m) + \cos(L_m - \theta)\cos(\delta_m)\cos(h_m) \tag{13}$$

The thermal resistance from PV cells to the fin sheet is calculated

$$R_{p-f} = R_p + R_{EVA} + R_{ei} = \frac{\delta_p}{k_p A_p} + \frac{\delta_{EVA}}{k_{EVA} A_p} + \frac{\delta_{ei}}{k_{ei} A_p} \tag{14}$$

The corresponding electricity output per unit area is defined

$$q_e = I(\tau_c \alpha)_p \beta_p \eta_{rc} \left[ 1 - \beta_{PV} (T_p - T_{rc}) \right] \tag{15}$$

### *3.3. One-dimensional unsteady-sate heat conductance of the fin sheet*

The time-dependent heat conductance on the PV-based fin sheet can be tackled as a typical one-dimensional unsteady-state heat transfer on an infinite flat-plate and its heat balance equations are expressed as

$$\begin{cases} \rho_f c_f \delta_f \dfrac{\partial T_f}{\partial \tau} = k_f \delta_f \dfrac{\partial^2 T_f}{\partial x^2} + \left(T_p - T_f\right) / R_{p-f} A_p - \left(T_f - T_a\right) / \left(R_{f-a} A_{fs} + 1 / h_a A_{fe}\right) \end{cases} \tag{16}$$

$$\rho_f c_f \delta_f \frac{\partial T_{f,11}}{\partial \tau} = \left(T_{p,11} - T_{f,11}\right) / R_{p-f} A_p - \left(T_{f,11} - T_{hp,w}\right) / R_{f-hp} A_{fc} - \left(T_{f,11} - T_a\right) / R_{f-a} A_{fs} \tag{17}$$

The initial temperature and boundary conditions are described

$$\begin{cases} T\left(x, 0\right) = T_{f,i}{}^{0}, \tau = 0 \\ -k_f \left.\dfrac{\partial T}{\partial x}\right|_{x=0} = h_a \left(T_{f,0} - T_a\right), \tau > 0 \\ T\left(\dfrac{W}{2}, \tau\right) = T_{f,11}, \tau > 0 \end{cases} \tag{18}$$

The thermal resistances of fin sheet insulation to air, and fin sheet to heat pipe external wall are respectively written by

$$R_{f-a} = \frac{\delta_{fs}}{k_{fs} A_{fs}} \tag{19}$$

$$R_{f-hp} = \frac{\delta_f}{k_f A_{fc}} \tag{20}$$

### *3.4. Heat balance equation of the loop heat pipe*

The heat balance equation for the loop heat pipe can be described as

$$\frac{1}{4}\pi\left(D_{hp,o}{}^{2} - D_{hp,in}{}^{2}\right)\rho_{hp} c_{hp} L_{hp} \frac{\partial T_{hp,w}}{\partial \tau} = \left(T_{f,11} - T_{hp,w}\right) / R_{f-hp} A_{fc} - \left(T_{hp,w} - T_{r,m}\right) / R_{hp-r} - \left(T_{hp,w} - T_a\right) / R_{hp-a} \tag{21}$$

$$R_{hp-a} = \frac{\ln\left(D_{hp,o} / D_{hp,in}\right)}{2\pi L_{hp} k_{hp}} + \frac{1}{h_a A_{hp}} \tag{22}$$

$$R_{hp-r} = R_{hp,w} + R_{wi} + R_{lf} + R_{hx} + R_r \tag{23}$$

$$R_{hp,w} = \frac{\ln\left(D_{hp,o} / D_{hp,in}\right)}{2\pi L_{hp} k_{hp}} \quad (24)$$

$$R_{wi} = \frac{\ln\left(D_{hp,in} / D_{v,e}\right)}{2\pi L_{wi} k_{wi}} \quad (25)$$

$$k_{wi} = \frac{k_l\left[\left(k_l + k_s\right) - \left(1-\varepsilon_{wi}\right)\left(k_l - k_s\right)\right]}{\left[\left(k_l + k_s\right) + \left(1-\varepsilon_{wi}\right)\left(k_l - k_s\right)\right]} \quad (26)$$

$$\varepsilon_{wi} = 1 - \frac{1.05\pi n_{wi} D_{wi}}{4} \quad (27)$$

$$R_{lf} = \frac{\ln\left[D_{hx,in} / \left(D_{hx,in} - 2\delta_{lf}\right)\right]}{2\pi L_{lf} k_{lf}\left(N_{hx}/2 - 1\right)} \quad (28)$$

$$R_{hx} = \frac{\ln\left(D_{hx,o} / D_{hx,in}\right)}{2\pi\left(H_{hx}/2\right) k_{hx}\left(n_{hx}/2 - 1\right)} \quad (29)$$

$$R_r = \frac{1}{h_r A_{hx,r}\left(N_{hx}/2\right)} \quad (30)$$

$$h_r = h_{r,l}\left[\left(1-x_r\right)^{0.8} + \frac{3.8 x_r^{0.76}\left(1-x_r\right)^{0.04}}{\mathrm{Pr}_r^{0.38}}\right] \quad (31)$$

$$h_{r,l} = \frac{Nu_{r,l} k_{r,l}}{D_{hx,in}} \quad (32)$$

$$Nu_{r,l} = 0.023\,\mathrm{Re}_{r,l}^{0.8}\,\mathrm{Pr}_{r,l}^{0.4} \quad (33)$$

$$\mathrm{Re}_{r,l} = \frac{m_r\left(1-x_r\right) D_{hx,in}}{A_{hx,r}\rho_{r,l}\nu_{r,l}\left(N_{hx}/2\right)} \quad (34)$$

$$\mathrm{Pr}_{r,l} = \frac{\mu_{r,l} c_{p,lr}}{k_{r,l}} \tag{35}$$

### *3.5. Heat balance equation of the heat pump cycle and water tank*

The solar heat delivered to the heat pump operation is theoretically given by

$$\frac{\partial \left( M_r H_{r,e} \right)}{\partial \tau} = \left( T_{hp,w} - T_{r,m} \right) / R_{hp-r} - \left( T_{hp,w} - T_a \right) / R_{hp-a} \tag{36}$$

The heat pump condenser heat is fully filled into the water, defined as

$$M_w c_w \frac{\partial T_w}{\partial \tau} = \frac{\partial \left( M_r H_{r,c} \right)}{\partial \tau} - \left( T_w - T_a \right) / R_{w-a} \tag{37}$$

$$R_{w-a} = \frac{\ln \left( D_{ws,o} / D_{ws,in} \right)}{2\pi L_{ws} k_{ws}} + \frac{1}{h_a A_w} \tag{38}$$

To numerically solve above equations, the time step, $\Delta\tau$, and space step, $\Delta x$, are respectively set at 1min and 22mm, the grouped energy derivation equations can be discretized using the forward and centre finite differential method. An initial temperature distribution ($\tau$=0) from module cover to water in tank will be assumed before starting iteration. The corresponding initial and boundary conditions are obtained from the experimental records.

### *3.6. Module efficiencies and system performance indicators*

The overall energy efficiency is yielded from the first law of thermodynamics and indicates the percentage of the energy converted from the solar radiation, defined as

$$\eta_e = \frac{\int_{\tau_0}^{\tau_{k+1}} Q_e d\tau}{\int_{\tau_0}^{\tau_{k+1}} A_m I d\tau} \tag{39}$$

$$\eta_{th} = \frac{\int_{\tau_0}^{\tau_{k+1}} Q_{th} d\tau}{\int_{\tau_0}^{\tau_{k+1}} A_m I d\tau} \tag{40}$$

$$\eta_o = \eta_e + \eta_{th} \tag{41}$$

The standard system performance coefficient (*COP*) is evaluated

$$COP = \frac{\int_{\tau_0}^{\tau_{k+1}} Q_w d\tau}{\int_{\tau_0}^{\tau_{k+1}} (Q_w - Q_{th}) d\tau} \quad (42)$$

As such PV/LHP system yields not only heat but also electricity, a comprehensive system coefficient of thermal-and-electrical performance ($COP_{PV/T}$) is defined, where the solar electricity is converted into the equivalent thermal energy through use of average electricity-generation efficiency (commonly 38% [Huang, 2001]) in a coal-fired power plant.

$$COP_{PV/T} = \frac{\int_{\tau_0}^{\tau_{k+1}} (Q_w + Q_e / 0.38) d\tau}{\int_{\tau_0}^{\tau_{k+1}} (Q_w - Q_{th}) d\tau} \quad (43)$$

To find out the discrepancy between the theoretical and experimental results, the root mean square percentage deviation (*RE*) will be evaluated using the following expression:

$$RE = \sqrt{\frac{\sum [100 \times (X_e - X_s) / X_e]^2}{N}} \quad (44)$$

*where*, $X_e$ and $X_s$ represents the experimental and simulated values respectively.

## 4. Results and discussion

To validate the computer simulation, the model was adjusted to the identical set-ups as for the outdoor conditions and system geometry/operational parameters. The discrepant results obtained from the comparison were put into calculation of the model accuracy. Further, dedicated analyses and discussions towards the modelling/testing results were conducted.

### *4.1. Experimental set up and testing*

A prototype of PV/LHP-HP system was constructed in Shanghai, China and run for testing under the practical outdoor conditions. The PV/LHP module, with an effective absorbing area of 0.612m$^2$, was fixed to the 30$^o$ tilted frame, and fitted with the single glazing cover on top. The PV cells, consisting of totally 36 (4 × 9 array) pieces each with sizes of 125 × 125 × 0.3 (mm × mm × mm), took up nearly 90% of the absorbing surface. Table 1 presents the values of the characteristic parameters relating to the PV cells under the standard testing conditions. When making up the PV lamination, a black 5052 aluminum alloy sheet, coated with 20μm anodic oxidation film to prevent electrical transmission, was used to replace the conventional TPT (tedlar-Polyester-tedlar) base-board of PV cells. A 5 mm thick aluminum Ω-type fin sheet, embracing a wicked pipe (with 160 x 60 copper meshes), was adhered to the PV base-board using silicon sealants. This pipe, connecting to the liquid and vapour transportation lines and condensing heat exchanger, formed up a loop that was evacuated and then filled

with 75ml of water/glycol mixture (95%/5%) as working fluid. Further, the system employed a 1kW-rating compressor with evaporation/condensation temperatures of 10°C/55°C, which was charged with 300g of R134a refrigerant. A 35-liter water tank with built-in cooper heat exchanging coils was also installed and connected to the heat pump. The electrical parts of the system include a 12V (10A) controller, 500W DC/AC inverter, a 100AH (12V) battery, and the connection wires. The insulation materials including the foamy polyurethane for piping and polystyrene board for exchangers were also applied to minimize the heat loss of the system components.

Table1: Characteristics of the PV module under standard testing conditions

| | |
|---|---|
| *At short-circuit current* | $I_{SC} = 5.54\ A,\ V_{SC} = 0\ V$ |
| *At open-circuit voltage* | $I_{OC} = 0\ A,\ V_{OC} = 22.32\ V$ |
| *At the maximum power point* | $I_{mp} = 4.89\ A,\ V_{mp} = 18.23\ V\ (P_{mp} = 89.1\ W,\ \eta_o = 16.8\%)$ |

The outdoor experiment was performed on 21st November 2011 in Shanghai, China (31°11'N and 121°29' E). The daily variation of solar radiation and ambient temperature are shown in Fig. 4. The initial water temperature in the tank was measure at around 14.38°C. The testing was operated from 8:40 to 16:20 and while testing, all the sensors/instruments were placed in the positions, and were linked to a DT500 data logger and then to a computer. The testing data were recorded every minute interval.

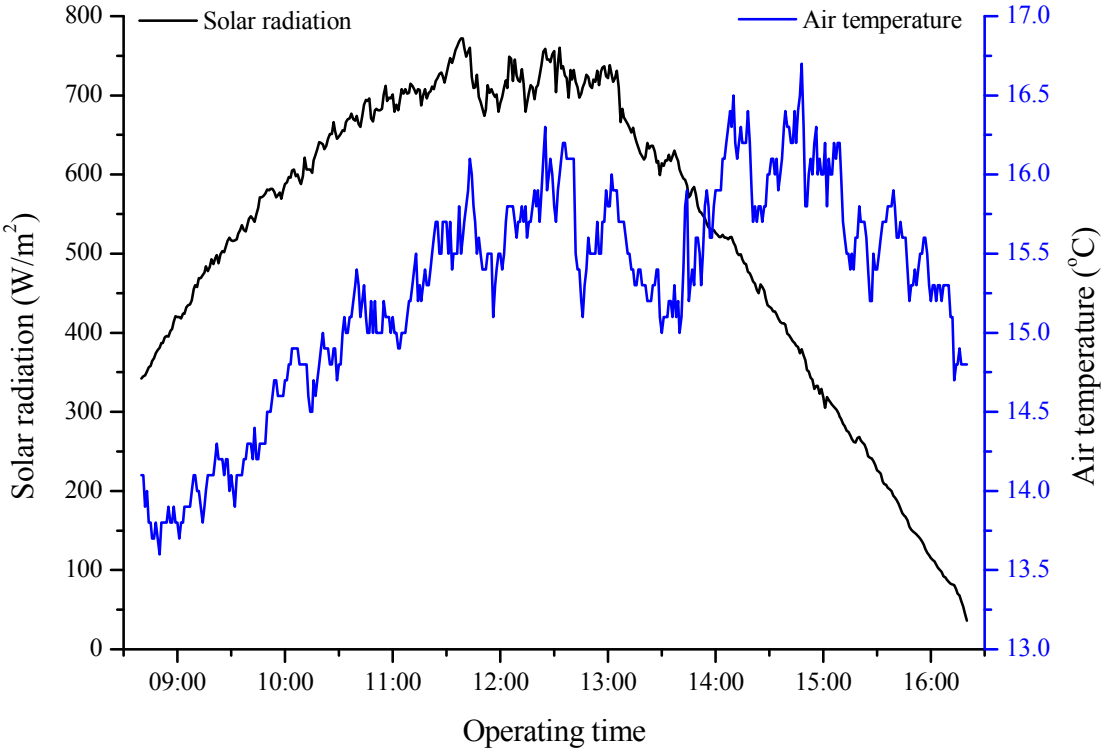


Fig. 4: Daily solar radiation and air temperature

### *4.2. Photovoltaic power output and module electrical energy efficiency*

Fig. 5 provided the comparison between modelling and testing results of the photovoltaic power and module electrical energy efficiency. The average modelling/testing solar electrical gain and the corresponding efficiencies were respectively 29.91W/29.45W and 9.23%/9.12%, giving an excellent mutual agreement with the mean deviation of 1.45%. The daily electrical yield was found quite similarly as the solar radiation to gradually increase in the morning while falling down significantly after it reached the peak value at noontime. The electrical energy efficiency was observed to slightly increase at the start-up stage and largely decreased at the end-up stage, while it remained relatively smooth during most of the testing period. The reason for the parabolic power curve was mainly due to the variation of solar radiation intensity and its incident angle. It is well known that stronger solar radiation and smaller incident angle of the solar beam would result in more absorbed solar energy and therefore higher solar electrical gain, which, during this experiment, ideally appears at the noontime and became less satisfactory in the morning and afternoon. The electrical energy efficiency usually changes oppositely with the solar incident angle and PV cells' temperature, and the ultimate electrical energy efficiency would be determined depending upon whose transient impact is greater. Normally, a lower PV temperature will appear in the early morning or late afternoon while the solar incident angle happens to be in the larger magnitude. For this dedicated testing, it's obvious that the solar incident angle was the primary governing factor in the early morning and later afternoon, resulting in the smaller electrical energy efficiency; while these two parameters became equivalent and cause less fluctuated electrical energy efficiency during rest operating period.

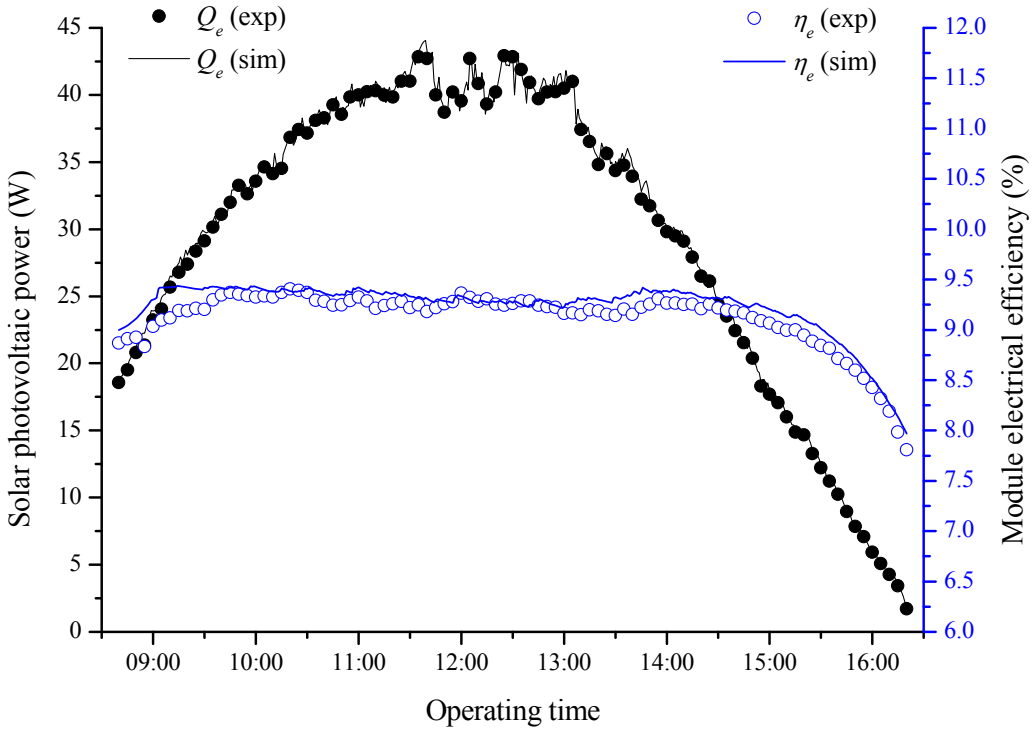


Fig. 5: Daily power output and module electrical energy efficiency versus operating time

### *4.3. Solar heat gain and module thermal energy efficiency*

Variation of both solar heat gain and module thermal energy efficiency versus the operating time was given in Fig. 6. The average modelling/testing solar heat and the corresponding thermal energy efficiencies were respectively about 122.87W/120.08W and 38.76%/38.13%,

giving a reasonable mutual agreement with the mean deviation of 5.20%. It is found the daily solar thermal yield also behaved a parabolic curve which sharply grew in the morning and performed a slightly-smooth declination after about 13:00 in the afternoon. The features of transient solar radiation and incident angle primarily affected the energy absorption of the module and also characterized its corresponding daily thermal performance. Meanwhile, as the air temperature nearly kept increasing most of the day, less heat loss will occur in the afternoon, enabling a relatively-smooth decrease of the solar heat gain. The module thermal energy efficiency was observed to sharply increase in both the start-up and end-up stages, and remained relatively steady during rest operating period. As the heat pump was run at a controlled evaporating temperature, this can be explained that when the system started to operate, the module-self warming up and lower surrounding air temperature would negatively reduced the instant evaporating heat gain of refrigerant and thus weakened the thermal energy efficiency; while in the operation end, the delayed warm module temperature and higher surrounding air temperature would positively enlarge the transient evaporating heat gain of refrigerant and therefore strengthened the thermal energy efficiency. During rest operation period, a less-fluctuated thermal efficiency can be obtained by reason of the stable refrigerant evaporating temperature and the equivalent overall functions of both solar incident angle and air temperature.

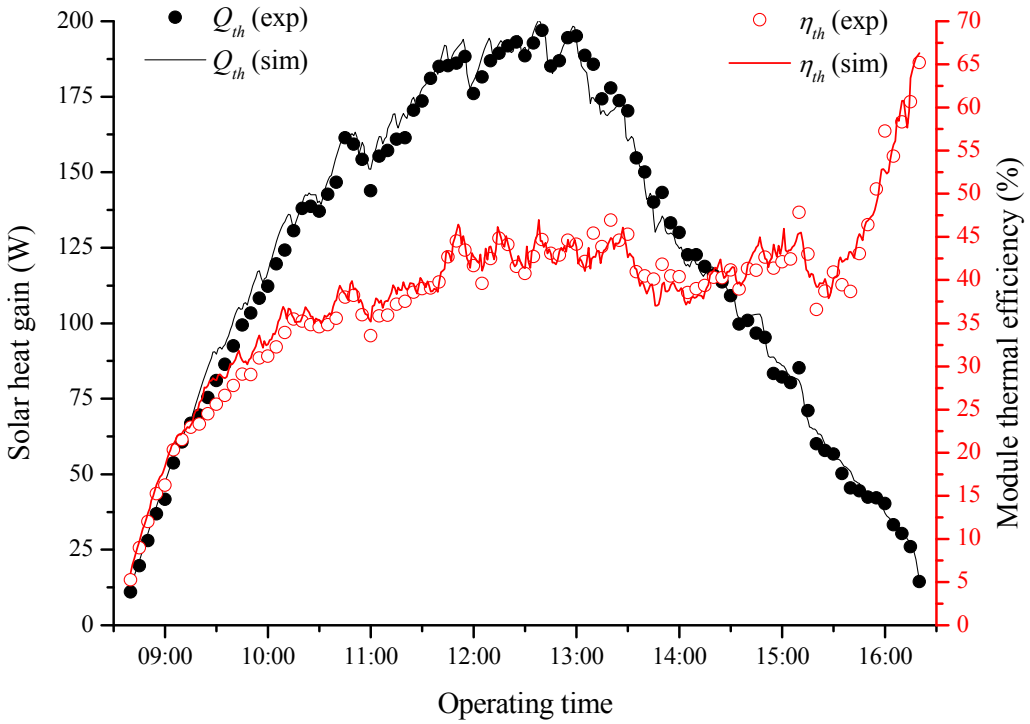


Fig. 6: Daily solar heat gain and module thermal energy efficiency versus operating time

### *4.4. Heat pump condensing capacity and system performances*

Fig. 7 illustrated the variation of daily heat pump condensing capacity, standard system performance coefficient (*COP*) and the overall performance coefficient of this hybrid system ($COP_{PV/T}$). The average modelling/testing results of water heat gain, *COP* and $COP_{PV/T}$ were respectively about 148.11W/146.86W, 5.88/5.51 and 9.28/8.81, giving the mutual agreements with the mean deviations of 4.58%, 8.80% and 9% respectively. The daily varying discipline of the heat pump condensing capacity was found nearly the same as that of the daily absorbed solar heat, as it was only upgraded by inputting the fixed compressor work. The typical *COP* values stayed nearly constant all the day in that the evaporating and condensing temperatures

of the heat pump cycle were set fixed. The $COP_{PV/T}$ of this hybrid prototype system was found to significantly decrease during the early half-hour operation, and then remained relatively stable. This is because in the early testing period, the electrical output was the primary impacting factor of $COP_{PV/T}$ at that time being, which was much larger than the system heat gain and resulted in the considerably high $COP_{PV/T}$ values; while with the rapid increase of system heat gain, the thermal yield, based on thermodynamic cycle of the heat pump, became the crucial impacting factor and caused the $COP_{PV/T}$ becoming much smaller and steady as close to the *COP*s. In this case, the electrical output was a positive addition to the system overall performance, and thus made the $COP_{PV/T}$ larger than typical *COP* values.

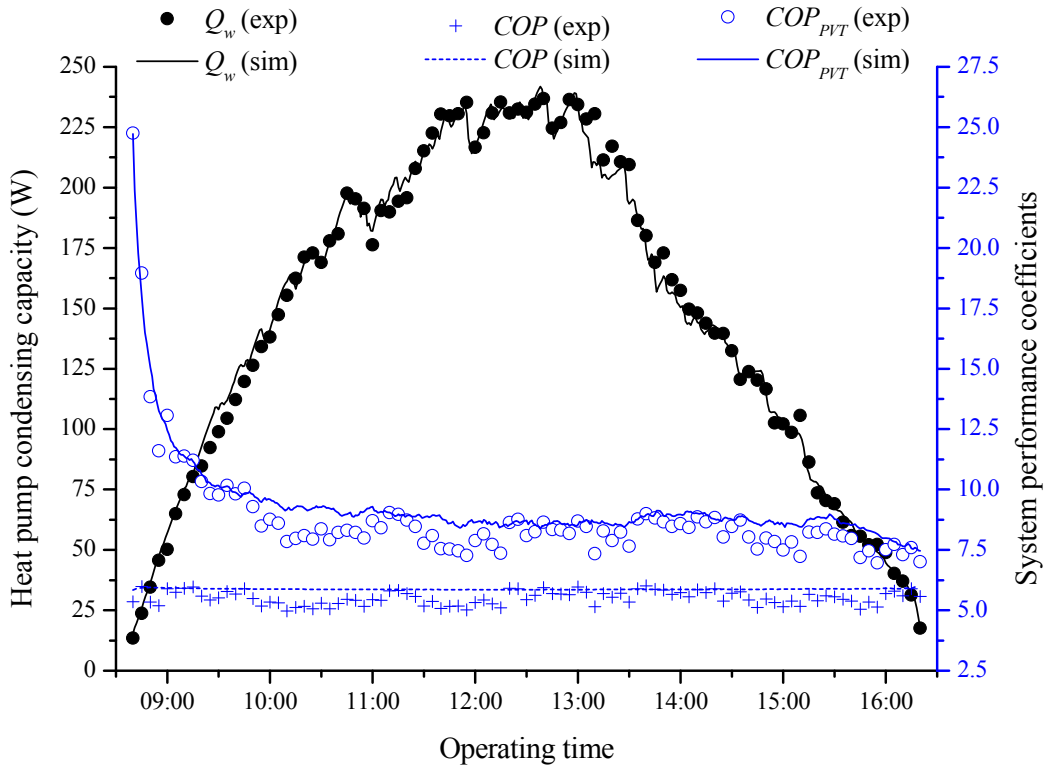


Fig. 7: Daily water heat gain and system performances versus operating time

It should be noted that as the heat pump compressor worked intermittently, the amount of the compressor electrical consumption were recorded every intermittent period and averagely divided by each interim time length. In this circumstance, the measured system *COP* and $COP_{PV/T}$ values appeared to be less accurate than other parameters.

### *4.5. Error analysis*

It has been found that certain differences were in existence between the modelling and testing results of the system's characteristic parameters, as indicating in Table 2. For all sets of comparison, the mean deviations were no larger than 9%, which were acceptable in terms of general engineering applications, and indicated that the established model can predict the system performance at a reasonable accuracy.

The minor discrepancy can be caused by both theoretical and measurement errors. For the theoretical analysis, some simplified assumptions and empirical formulas were made and utilized, such as inappropriate omissions of heat capacities of two EVA layers, ignorance of the isentropic efficiency of heat pump compressor, may be the potential reasons for error

generation. During the measurement, the factors, like insufficient insulations, inaccurate instrument/sensors, may cause the deviation of testing figures from prediction.

Table 2: Daily average system performances

| *Results* | *I (W)* | $Q_e$ *(W)* | $Q_{th}$ *(W)* | $Q_w$ *(W)* | $\eta_e$ *(%)* | $\eta_{th}$ *(%)* | $\eta_o$ *(%)* | *COP* | $COP_{PV/T}$ |
|---|---|---|---|---|---|---|---|---|---|
| *Experiment* | *321.44* | *29.45* | *120.08* | *146.86* | *9.12* | *38.13* | *47.24* | *5.51* | *8.81* |
| *Simulation* | | *29.91* | *122.87* | *148.11* | *9.23* | *38.76* | *47.99* | *5.88* | *9.28* |
| *Error (RE)* | | *1.45%* | *5.20%* | *4.58%* | *1.45%* | *5.20%* | *4.00%* | *8.80%* | *9.00%* |

### *4.6. Comparison between PV/LHP-HP system and conventional solar/air energy systems*

Given above outdoor weather conditions, system geometry and operational parameters, the daily average modelling and testing results were put into comparison with the conventional solar/air energy systems, displayed in Fig.8. It was observed that the mean overall efficiency of the PV/LHP module was more than 47%, which was higher than the average operational values of the independent PV panels (around 10%-12% [Solardirect, 2012]) and standard solar thermal collectors (about 40% [Bigginhill, 2012]). The system performance indicators (*COP* and $COP_{PV/T}$) were receptively found nearly twice and fourfold of the conventional air-source heat pump water heating system (ASHP) [Wikipedia, 2012], whilst one-and-a-half times and twice over the integral-type solar-assisted heat pump system (ISAHP) [Huang et al., 2001].

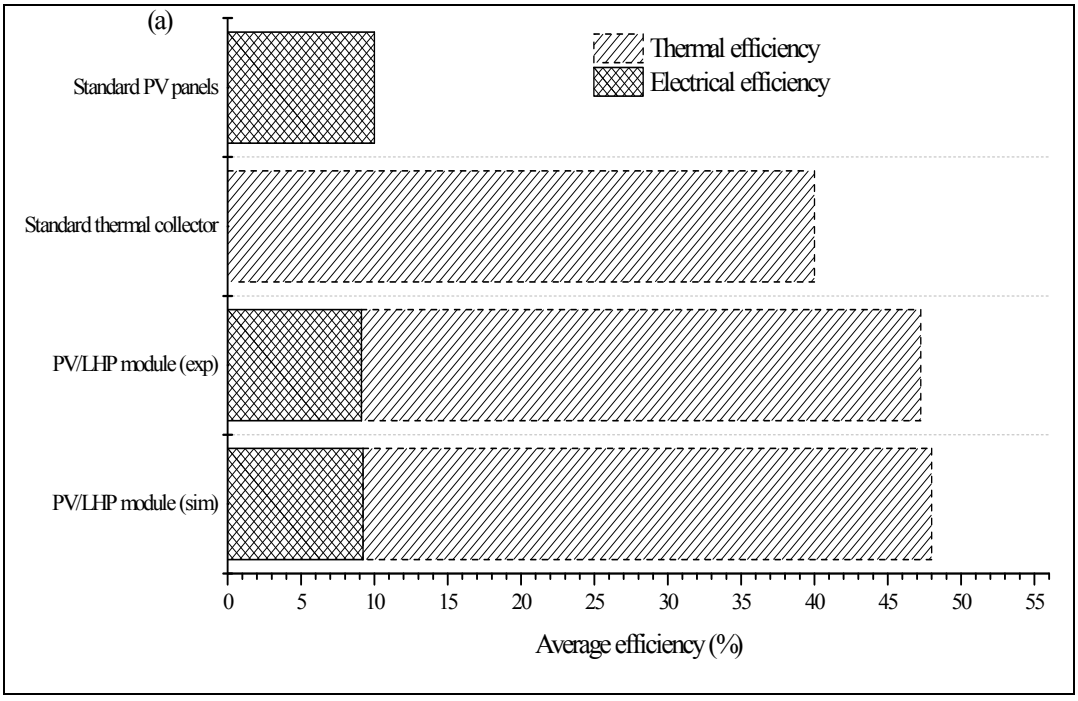

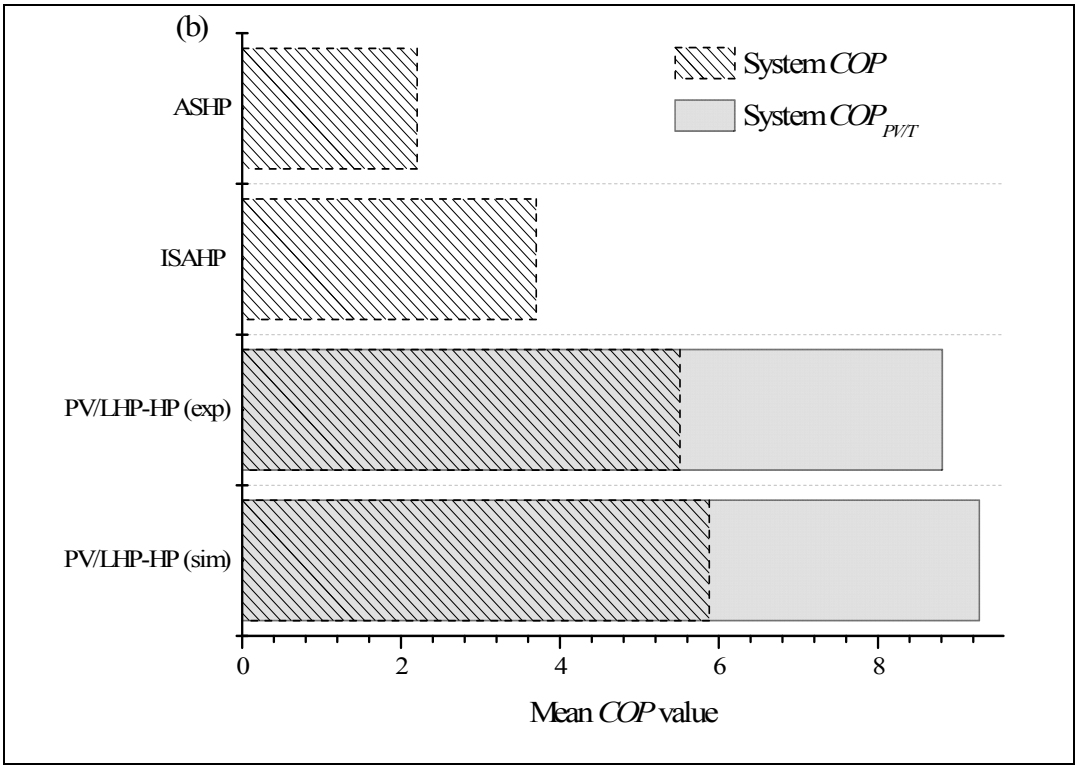


Fig. 8: Comparison between the PV/LHP-HP system and (a) independent PV panels, standard solar thermal collectors and (b) conventional air-source and solar-assisted heat pump water heating systems

## 5. Conclusion

This paper reported the daily dynamic performance of a novel solar photovoltaic/loop-heat-pipe heat pump water heating system, which has the potential to overcome some difficulties remaining in the existing PV/T technologies. A dedicated computer model was developed to predict the system performance depending upon heat balances mechanism. A prototype system was constructed and tested to examine its characteristic behaviors under practical outdoor weather conditions. Parallel comparison between the modelling and experimental results indicated that these two sets of data were in good agreement, and thus the established model was able to predict the system performance at a reasonable accuracy (mean error less than 9%). It was found that the average electrical/heat gain and efficiencies of the module were measured at around 29.45W/120.08W and 9.12%/38.13% respectively. For the system performance, testing results showed the average heat pump condensing capacity, values of *COP* and $COP_{PV/T,}$ were at around 146.86W, 5.51 and 8.81 respectively. Error analysis was conducted from both the theoretical and experimental aspects. This hybrid technology enables the higher overall solar-energy conversion efficiency than the independent solar photovoltaic panel and solar thermal collector. The coefficients of system performance were nearly 1.5-4 times over the conventional solar/air heat pump water heating systems.

In overall, the research provided a dedicated method to determine the dynamic performance of such a new PV/LHP-HP system and gave some useful clues on further optimization of heat-pipe-type PV/T technologies and solar driven (space and hot water) heating systems, which would obviously contribute to realization of the energy saving and associated carbon emission targets set for buildings globally.

## Nomenclature

| | |
|---|---|
| $A$ | *area ($m^2$)* |
| $c$ | *Specific heat capacity (J/kg K)* |
| $D$ | *diameter (m)* |
| $h$ | *heat transfer coefficient (W/m K)* |
| $h_m$ | *hour angle (rad)* |
| $H$ | *thermal enthalpy (kJ/kg); height (m)* |
| $I$ | *solar radiation ($W/m^2$)* |
| $k$ | *thermal conductivity ($W/m^2$ K)* |
| $K$ | *extinction coefficient of cover* |
| $L$ | *length (m)* |
| $L_m$ | *local latitude* |
| $m$ | *mass flow rate (kg/s)* |
| $M$ | *mass (kg)* |
| $n$ | *mesh number* |
| $n_g$ | *ratio of refraction index* |
| $Nu$ | *Nusselt number* |
| $q$ | *unit energy rate ($W/m^2$)* |
| $Q$ | *energy rate (W)* |
| $Pr$ | *Prandtl number* |
| $R$ | *thermal resistance (K/W)* |
| $Ra$ | *Rayleigh number* |
| $Re$ | *Renault number* |
| $T$ | *temperature (K)* |
| $V$ | *velocity (m/s)* |
| $W$ | *width (m)* |
| $x$ | *width parameter* |
| $x_r$ | *refrigerant saturation rate* |

### *Greek*

| | |
|---|---|
| $\alpha$ | *absorption ratio* |
| $\beta_p$ | *PV packing factor* |
| $\beta_{PV}$ | *efficiency temperature coefficient* |
| $r_{\|\|}/r_{\perp}$ | *parallel/perpendicular components of unpolarized radiation for surfaces* |
| $\delta$ | *thickness (m)* |
| $\delta_m$ | *declination angle (rad)* |
| $\varepsilon$ | *emissivity; porosity* |
| $\eta$ | *efficiency* |
| $\theta$ | *collector slop (degree)* |
| $\theta_1$ | *incidence angle (rad)* |
| $\theta_2$ | *angle of direct solar beam (rad)* |
| $\mu$ | *dynamic viscosity (kg/m s)* |
| $\nu$ | *kinematic viscosity ($m^2/s$)* |
| $\rho$ | *density ($kg/m^3$)* |
| $\sigma$ | *Stefan–Boltzman constant* |
| $\tau_c$ | *cover transmittance* |
| $\tau_{c,a}$ | *transmittance due to absorption* |

### *Subscripts*

| | |
|---|---|
| *a* | *air* |
| *b* | *backplane* |
| *c* | *cover; convection* |
| *e* | *electricity* |
| *ei* | *electrical insulation* |
| *f* | *fin sheet* |
| *fc* | *center of fin sheet* |
| *fe* | *edge of fin sheet* |
| *fs* | *insulation around fin sheet* |
| *hp* | *heat pipe* |
| *hp,w* | *heat pipe wall* |
| *hx* | *heat exchanger* |
| *l* | *liquid* |
| *lf* | *liquid film* |
| *m* | *mean, module* |
| *p* | *PV* |
| *r* | *refrigerant* |
| *r,e* | *refrigerant evaporator* |
| *r,l* | *liquid refrigerant* |
| *rc* | *reference temperature* |
| *r,m* | *mean refrigerant* |
| *R* | *radiation* |
| *s* | *solid* |
| *th* | *thermal* |
| *o* | *overall* |
| *v,e* | *vapour core in evaporator* |
| *w* | *water* |
| *wi* | *wick* |
| *ws* | *insulation of water tank* |
| *ws,in* | *inner tank insulation* |
| *ws,o* | *outer tank insulation* |

**References:**

EU energy and transport in figures, statistical pocket book 2007/2008.

Zondag HA et al., 2002, The thermal and electrical yield of a PV-Thermal collector, Solar Energy Vol. 72(02), pp.113–28.

X Zhang et al., 2012, Review of R&D progress and practical application of the solar photovoltaic/thermal (PV/T) technologies, Renewable and Sustainable Energy Reviews, Vol. 16(01), pp. 599-617.

A. Faghri, 1995, Heat Pipe Science and Technology (1st edition), Taylor & Francis Group.

Huang B. J et, al., 2001, Performance evaluation of solar photovoltaic/thermal systems. Solar Energy 70: 443-448.

Solar photovoltaic modules, < http://www.solardirect.com/pv/pvlist/pvlist.htm>, accessed on 12-03-2012

Solar water heating collector, < http://www.bigginhill.co.uk/solar.htm>, accessed on 12-03-2012

Heat pump technology, <http://en.wikipedia.org/wiki/Heat_pump>, accessed on 12-03-2012

B.J. Huang et al., 2001, Performance characteristics of integral type solar assisted heat pump, Solar Energy, Vol. 71 (06), pp. 403–414.